HHS Public Access

Author manuscript

*Cell Rep*. Author manuscript; available in PMC 2016 March 09.

Published in final edited form as:

*Cell Rep*. 2016 March 8; 14(9): 2041–2049. doi:10.1016/j.celrep.2016.02.011.

# Reciprocal Degradation of YME1L and OMA1 Adapts Mitochondrial Proteolytic Activity During Stress

**T. Kelly Rainbolt**, **Justine Lebeau**, **Cristina Puchades**, and **R. Luke Wiseman***

Department of Molecular & Experimental Medicine, Department of Chemical Physiology, The Scripps Research Institute, La Jolla, CA 92037

## SUMMARY

The mitochondrial inner membrane proteases YME1L and OMA1 are critical regulators of essential mitochondrial functions including inner membrane proteostasis maintenance and mitochondrial dynamics. Here, we show that YME1L and OMA1 are reciprocally degraded in response to distinct types of cellular stress. OMA1 is degraded through a YME1L-dependent mechanism in response to toxic insults that depolarize the mitochondrial membrane. Alternatively, insults that depolarize mitochondria and deplete cellular ATP stabilize active OMA1 and promote YME1L degradation. We show that the differential degradation of YME1L and OMA1 alters their proteolytic processing of the dynamin-like GTPase OPA1, a critical regulator of mitochondrial inner membrane morphology, which influences the recovery of tubular mitochondria following membrane depolarization-induced fragmentation. Our results reveal the differential stress-induced degradation of YME1L and OMA1 as a mechanism to sensitively adapt mitochondrial inner membrane protease activity and function in response to distinct types of cellular insults.

## INTRODUCTION

Mitochondrial inner membrane proteases regulate essential functions including electron transport chain activity, mitochondrial inner membrane proteostasis maintenance and mitochondrial dynamics (Anand et al., 2013; Quiros et al., 2015). Imbalances in the activity of these proteases can lead to pathologic mitochondrial dysfunction and are implicated in the onset and pathology of many diseases (Rugarli and Langer, 2012). As such, mitochondrial inner membrane proteases must be regulated to adapt mitochondrial proteolytic activity to specific cellular demands and environmental challenges.

*Corresponding author: R. Luke Wiseman, Department of Molecular & Experimental Medicine, Department of Chemical Physiology, 10550 N. Torrey Pines Rd. MEM 220, The Scripps Research Institute, La Jolla, CA 92037, Phone: (858) 784-8820, Fax: (858) 784-8891, wiseman@scripps.edu.

**AUTHOR CONTRIBUTIONS**

TKR and JL conceived, designed, and carried out experiments and interpretation of the data. CP carried out experiments. RLW supervised the project. All authors were involved in the drafting and revision of the manuscript.

Additional Experimental Procedures are included in the Supplemental Information.

Two mitochondrial proteases that regulate proteostasis in the inner membrane and intermembrane space (IMS) are the ATP-independent protease OMA1 and the ATP-dependent AAA+ protease YME1L. These proteases assemble as homooligomers in the inner membrane with their active sites oriented towards the IMS (Baker et al., 2014; Stiburek et al., 2012). YME1L is constitutively active. Conversely, OMA1 is maintained in a quiescent state in the absence of stress and is activated in response to cellular insults such as mitochondrial membrane depolarization (Baker et al., 2014; Zhang et al., 2014). YME1L and OMA1 have many independent functions (Bohovych et al., 2015; Desmurs et al., 2015; Jiang et al., 2014; Li et al., 2015; Rainbolt et al., 2013; Stiburek et al., 2012). However, these proteases coordinate to regulate mitochondrial morphology through their differential processing of the dynamin-like GTPase OPA1 (Anand et al., 2014). YME1L-dependent OPA1 processing promotes tubular mitochondrial morphology, while OMA1-dependent OPA1 processing induces mitochondrial fragmentation (Anand et al., 2014; Mishra et al., 2014; Quiros et al., 2012). Mitochondrial morphology influences many aspects of mitochondrial biology including ETC activity, apoptotic sensitivity, and mitophagy (Chan, 2012). Thus, the regulation of mitochondrial morphology afforded by differential YME1L- and OMA1-dependent OPA1 processing is a key determinant in dictating mitochondria function.

YME1L and OMA1 have both been shown to be stress-sensitive mitochondrial proteases (Baker et al., 2014; Rainbolt et al., 2015; Zhang et al., 2014). This suggests that the activity of these proteases could be regulated to adapt mitochondrial function to specific types of cellular stress. Here, we show that YME1L and OMA1 are reciprocally degraded in response to distinct types of toxic insults. OMA1 is degraded through a YME1L-dependent mechanism following insults that depolarize mitochondria. Alternatively, YME1L is degraded in response to insults that depolarize mitochondria and deplete cellular ATP through a mechanism involving OMA1 (Rainbolt et al., 2015). Furthermore, we show that the differential degradation of YME1L and OMA1 alters their proteolytic processing of OPA1 and influences the recovery of mitochondrial morphology following stress-induced fragmentation. Our results reveal that differential stress-induced YME1L and OMA1 degradation is a mechanism for cells to sensitively adapt mitochondrial inner membrane proteolytic activity and influence aspects of mitochondrial biology in response to distinct types of stress.

## RESULTS & DISCUSSION

### OMA1 degradation, but not activation, is ATP-dependent

OMA1 protease activation and degradation is proposed to be a coupled process that suppresses ATP-independent OMA1 protease activity following an acute insult (Baker et al., 2014). To test this prediction, we monitored OMA1 activity and degradation in mitochondria isolated from SHSY5Y cells. Mitochondria incubated in the absence of ATP did not show reductions in OMA1 protein levels (Fig. 1A). However, the OMA1 protease was activated as shown by increased OPA1 processing from a mixed population of long and short isoforms (t = 0 h) to only short isoforms (t = 6h), which is a process dependent on OMA1 (Rainbolt et al., 2015). In contrast, the addition of ATP reduced OMA1 in isolated

mitochondria, but did not affect OMA1-dependent OPA1 processing. This suggests that OMA1 degradation, but not OMA1 activation, is dependent on ATP.

OMA1 degradation is also dependent on ATP in cells. Endogenous OMA1 levels are rapidly reduced ($t_{1/2}$ = 1 h) in SHSY5Y cells treated with carbonyl cyanide *m*-chlorophenylhydrazone (CCCP; Fig. 1B,C) – a protonophore that depolarizes mitochondria but does not influence cellular ATP (Fig. S1A). OMA1 is activated under this condition as evidenced by the complete processing of OPA1 from long to short isoforms (Baker et al., 2014; Zhang et al., 2014). The addition of the translation inhibitor cycloheximide (CHX) alone does not significantly influence OMA1 levels, indicating that CCCP-dependent reductions in OMA1 reflect increased degradation (Fig. S1B). CCCP-induced OMA1 degradation is inhibited by co-addition of the glycolysis inhibitor 2-deoxy-D-glucose (2-DG; Fig. 1B,C) – a treatment that depolarizes mitochondria and reduces cellular ATP (Fig S1A). OMA1-dependent OPA1 processing was not affected by co-addition of CCCP and 2-DG, indicating that OMA1 was activated by this treatment. The ATP-dependence of membrane depolarization induced OMA1 degradation is also evident in SHSY5Y cells cultured in galactose supplemented media (SHSY5Y$^{GAL}$) treated with CCCP or the complex III inhibitor antimycin – A two treatments that depolarize mitochondria and deplete ATP in SHSY5Y$^{GAL}$ cells (Fig. S1C,D). In both treatments, we observe OMA1-dependent OPA1 processing, but incomplete OMA1 degradation (Fig. 1D,E & Fig S1E,F). Interestingly, these treatments induce the accumulation of a short OMA1 fragment (s-OMA1) previously shown to retain proteolytic activity (Zhang et al., 2014). Treatment of SHSY5Y$^{GAL}$ cells with the ATP synthase inhibitor oligomycin A, which hyperpolarizes the mitochondrial membrane and reduces cellular ATP (Fig. S1C), also modestly induces OPA1 processing, but does not induce complete OMA1 degradation (Fig. 1D,E). These results indicate that OMA1 degradation, but not OMA1-mediated OPA1 processing, is dependent on ATP in isolated mitochondria and living cells.

## ATP availability dictates YME1L and OMA1 stability following membrane depolarization

The above results show that membrane depolarization induced OMA1 degradation is inhibited by ATP depletion. YME1L degradation is induced by cellular insults that depolarize mitochondria and deplete ATP with a $t_{1/2}$ of ~3 h (Rainbolt et al., 2015). This suggests that the stabilities of these two proteases are differentially sensitive to insults that depolarize mitochondria in a process dictated by ATP availability. Consistent with this prediction, YME1L and OMA1 are differentially degraded in isolated mitochondria incubated in the absence or presence of ATP, respectively (Fig. 1A). The addition of CCCP or antimycin A to SHSY5Y$^{GAL}$ cells also induces YME1L degradation, while only modestly affecting OMA1 (Fig. 1D,E & Fig. S1E,F). Treatment of SHSY5Y$^{GAL}$ cells with oligomycin A alone does not induce YME1L degradation, reflecting the dependence of this process on membrane depolarization (Fig. 1D,E). YME1L and OMA1 are also differentially degraded in SHSY5Y cells cultured in glucose-supplemented media and treated with CCCP +/− 2-DG (Fig. 1F and Fig. S1G). Importantly, OMA1 is activated under all these conditions as evident by efficient OPA1 processing. Oxidative insults that deplete ATP and damage the mitochondrial membrane such as $H_2O_2$ also induce degradation of YME1L, but not activated OMA1 (Rainbolt et al., 2015). Similarly, YME1L is destabilized, while OMA1

remains stable, in mice subjected to hypoxic-ischemic (HI) injury, a pathologic condition that depletes cellular ATP and induces mitochondrial dysfunction (Baburamani et al., 2015).

These results indicate that YME1L and OMA1 are differentially degraded in response to cellular insults that depolarize mitochondria through a mechanism dictated by ATP availability (Fig. 1G). In the presence of ATP, membrane depolarization promotes the degradation of activated OMA1. Alternatively, in the absence of ATP, membrane depolarization stabilizes activated OMA1 and promotes YME1L degradation.

## Membrane depolarization induced degradation of activated OMA1 requires YME1L

CCCP-induced OMA1 degradation is predicted to occur through an autocatalytic mechanism (Baker et al., 2014; Zhang et al., 2014). We tested this prediction in isolated mitochondria. ATP-dependent OMA1 degradation in isolated mitochondria is inhibited by the addition of the zinc chelator *o*-phenanthroline *(o*-phe) (Fig. 2A) – an inhibitor of zinc metalloproteases such as OMA1 and YME1L. The inhibition of OMA1 activity by *o*-phe is shown by the impaired OPA1 processing. The addition of the non-hydrolyzable ATP analog AMP-PNP similarly inhibited degradation of OMA1, but did not influence OMA1-dependent OPA1 processing. This indicates that the OMA1 protease is active, but no autocatalytic degradation is observed. These results suggest that activated OMA1 is degraded in response to membrane depolarization through a mechanism involving an ATP-dependent zinc metalloprotease. One mitochondrial protease that fits this profile is YME1L. Stress-induced YME1L degradation involves active OMA1(Rainbolt et al., 2015). Thus, we evaluated whether OMA1 degradation involves YME1L

Depletion of *YME1L* in SHSY5Y cells increases basal OMA1 levels (Fig. S2A) and inhibits CCCP-induced OMA1 degradation (Fig. 2B,C). OMA1-dependent OPA1 processing is not affected in *YME1L*-depleted SHSY5Y cells treated with CCCP. Identical results were observed in SHSY5Y cells expressing an alternative *YME1L* shRNA and in *YME1L*-depleted HEK293T cells (Fig. S2B,C). ATP-dependent OMA1 degradation was also attenuated in mitochondria isolated from *YME1L*-depleted SHSY5Y cells (Fig. S2D). The expression of RNAi-resistant wild type YME1L ($YME1L^{WT}$) partially rescued the CCCP-induced OMA1 degradation in *YME1L*-depleted cells (Fig. S2E,F). The incomplete rescue of OMA1 degradation in these cells likely reflects the lower levels of exogenous YME1L as compared to controls. Overexpressing the ATPase deficient E382Q Walker B YME1L mutant ($YME1L^{WB}$) or the protease inactive E543Q YME1L mutant ($YME1L^{PI}$) showed no rescue of OMA1 degradation in *YME1L*-depleted cells (Fig. S2E,F). These results indicate that membrane-depolarization induced OMA1 degradation requires YME1L. Interestingly, membrane depolarization appears to be required for OMA1 degradation, as no significant OMA1 degradation is observed in CHX-treated cells in the absence of CCCP (Fig. S1B). This indicates that YME1L preferentially degrades activated OMA1 following membrane depolarization.

Our results suggest that YME1L is involved in the degradation, but not activation, of OMA1. We further tested this prediction using an overexpressed C-terminal HA-tagged OMA1. OMA1 activation can be followed by monitoring the autocatalytic processing of C-terminal tags on OMA1 (Baker et al., 2014; Zhang et al., 2014). This is evident, as

overexpression of a catalytically inactive E328Q OMA1$^{HA}$ slows the loss of HA-tagged protein in SHSY5Y cells treated with CCCP and SHSY5Y$^{GAL}$ cells treated with antimycin A (Fig. 2D,E). The reduced rate of E328Q OMA1$^{HA}$ loss observed in these cells likely reflects processing of the C-terminal HA tag in trans by the endogenous OMA1 also present in these cells. *YME1L*-depletion does not influence the autocatalytic processing of the C-terminal HA-tag on overexpressed wild-type OMA1$^{HA}$ in CCCP-treated cells (Fig. 2F). This indicates that YME1L is not required for OMA1 activation.

The above results suggest a model whereby membrane-depolarization induced OMA1 degradation proceeds through a two-step mechanism (Fig. 2G). First, membrane depolarization activates the OMA1 protease, allowing rapid processing of OMA1 substrates such as OPA1. This activation likely involves autocatalytic processing of the OMA1 protease, explaining previous results showing a dependence of OMA1 degradation on OMA1 protease activity (Baker et al., 2014; Zhang et al., 2014). Second, activated OMA1 is degraded through a mechanism involving ATP-dependent YME1L activity.

## ATP depletion slows the recovery of tubular mitochondria following membrane depolarization

YME1L and OMA1 coordinate to regulate mitochondrial morphology through their differential processing of the dynamin-like GTPase OPA1 (Anand et al., 2014). OPA1 can be expressed from 8 distinct mRNA transcripts that contain a single OMA1 cleavage site or both OMA1 and YME1L cleavage sites (Ishihara et al., 2006; Song et al., 2007). YME1L and OMA1 process OPA1 to yield a balance of 5 OPA1 isoforms – the long, uncleaved OPA1 isoforms *a* and *b* and the short, cleaved OPA1 isoforms *c*, *d* and *e* (Fig. 3A). YME1L constitutively cleaves long OPA1 to create the *d* isoform, which promotes the maintenance of tubular mitochondrial morphology (Mishra et al., 2014). Alternatively, stress-activated OMA1 processes all long OPA1 isoforms to the short *c* and *e* isoforms that promote mitochondrial fragmentation (Quiros et al., 2012). This indicates that differential stress-sensitivities of YME1L and OMA1 could influence the distribution of OPA1 isoforms and mitochondrial morphology following acute insults.

We tested this prediction by monitoring the distribution of OPA1 isoforms and mitochondrial morphology in cells following a pretreatment with CCCP +/− 2-DG. This pretreatment will induce alterations in activated OMA1 and YME1L through their differential degradation. Both treatments resulted in complete OMA1-dependent processing of long OPA1 isoforms to the *c* and *e* isoforms in SHSY5Y cells (Fig. 3A,B; t = 0 h recovery). The fraction of the YME1L-dependent OPA1 isoform *d* was not affected by either pretreatment. The loss of long OPA1 isoforms and the accumulation of the OMA1-dependent *c* and *e* isoforms should promote mitochondrial fragmentation. As expected, MEF cells stably expressing a mitochondrial-targeted GFP ($^{mt}$GFP) pretreated with CCCP or CCCP + 2-DG show identical levels of mitochondrial fragmentation (Fig. 3C,D; t=0 h recovery).

In contrast, the relative accumulation of OPA1 isoforms following a 6 h recovery from acute pretreatment with CCCP +/− 2-DG show differences. Pretreatment with CCCP + 2-DG decreased the recovery of the long OPA1 isoforms, relative to pretreatment with CCCP

alone (Fig. 3A,B). Moreover, the relative recovery of OMA1-dependent OPA1 isoforms *c* and *e* are increased following pretreatment with CCCP + 2-DG. The decreased levels of long OPA1 isoforms and the increased levels of the *c* and *e* OPA1 isoforms observed during the recovery from a CCCP + 2-DG pretreatment should impair the restoration of tubular mitochondrial morphology following stress-induced fragmentation. Consistent with this prediction, we observe reduced levels of tubular mitochondria and higher levels of fragmented mitochondria in MEF cells stably expressing $^{mt}$GFP pretreated with CCCP + 2-DG and allowed to recover for 2, 4 or 6 h when compared to the same timecourse of recovery following pretreatment with CCCP alone (Fig. 3C,D). This suggests that the recovery of tubular mitochondrial morphology following an acute insult that depolarizes mitochondria and depletes ATP is delayed through a mechanism that could involve alterations in OMA1- and YME1L-dependent OPA1 processing.

## The differential stress-sensitivity of YME1L and OMA1 alters OPA1 processing during recovery from acute membrane depolarization

Many factors could contribute to the altered distribution of OPA1 isoforms following acute insults that depolarize mitochondria and deplete ATP. While mitochondria membrane polarity is rapidly restored during recovery from pretreatment with CCCP or CCCP + 2-DG (Fig. S3A), the recovery of ATP levels are modestly delayed in SHSY5Y cells pretreated with CCCP + 2-DG (Fig. S3B). This delay could influence OPA1 synthesis and reduce the population of long isoforms imported into mitochondria during recovery from acute insult. [$^{35}$S]-metabolic labeling confirmed that pretreating cells with CCCP + 2-DG reduced the population of newly synthesized OPA1 following a 6 h recovery by 40% (Fig. 4A,B). CCCP pretreatment also reduced recovery of newly synthesized OPA1 by 20%. These reductions in newly synthesized OPA1 do not reflect a global reduction in protein synthesis, as the recovery of total [$^{35}$S]-labeled proteins is not significantly affected by either treatment (Fig. S3C). This indicates that the reduction in OPA1 synthesis involves other factors such as altered *OPA1* transcription or impaired OPA1 import into mitochondria.

The distribution of short OPA1 isoforms could also be influenced by the differential degradation of YME1L and active OMA1 induced by the CCCP +/− 2-DG pretreatment. The contributions of YME1L or OMA1 degradation on OPA1 processing and the recovery of tubular mitochondrial morphology cannot be ascertained using genetic approaches. *YME1L* depletion inhibits processing of OPA1 to the short *d* isoform and induces mitochondrial fragmentation in the absence of stress (Anand et al., 2014; Stiburek et al., 2012). Alternatively, *OMA1* depletion inhibits membrane-depolarization induced OPA1 processing and mitochondrial fragmentation (Anand et al., 2014; Quiros et al., 2012; Zhang et al., 2014). However, the impact of stress-induced YME1L or OMA1 degradation on OPA1 processing during recovery from an acute insult can be quantified using the assay shown in Fig. 4A. YME1L activity can be quantified by monitoring the fraction of [$^{35}$S]-labeled OPA1 isoform *d* (a YME1L product) following the 6 h recovery. Alternatively, OMA1 activity can be quantified by monitoring the fraction of [$^{35}$S]-labeled OPA1 isoform *c* (an OMA1 product) following a 6 h recovery. We were unable to quantify OMA1-dependent formation of isoform *e* due to low signal for this particular isoform and interference from a non-specific background band.

Using this approach, we found that the differential degradation of YME1L or OMA1 influences proteolytic processing of newly synthesized OPA1. The fraction of YME1L-dependent OPA1 isoform *d* decreases 50% following CCCP + 2-DG pretreatment when compared with recovery from CCCP pretreatment alone (Fig. 4A,C). This is consistent with the YME1L degradation observed following this treatment (Fig. 1F) (Rainbolt et al., 2015). Conversely, the fraction of the OMA1-dependent OPA1 isoform *c* increases 2-fold following pre-treatment with CCCP + 2-DG (Fig. 4A,D). This is consistent with the stabilization of activated OMA1 under these conditions (Fig. 1F). Surprisingly, the relative fraction of the newly synthesized long OPA1 isoforms *a* and *b* were not significantly affected following either pretreatment (Fig. S3D,E). This indicates that the total amount of newly synthesized OPA1 processed by either YME1L or OMA1 is not influenced by the degradation of these proteases. However, our results indicate that the differential degradation of these proteases dictates the processing of OPA1 to the pro-fusion isoform *d* or the pro-fragmentation isoform *c*.

Surprisingly, the levels of OMA1-dependent OPA1 processing observed following pretreatment with CCCP + 2-DG is less than that observed when CCCP is added to [$^{35}$S]-labeled cells 30 min prior to harvest (Fig. 4A,D, CCCP control). This could reflect the degradation of OMA1 during the recovery from CCCP + 2-DG afforded by the small amount of remaining YME1L. Consistent with this prediction, OMA1 levels decrease 60% during the 6 h recovery from CCCP + 2-DG pretreatment (Fig. 4E,F). This decrease appears to result from the loss of the s-OMA1 cleavage product, as opposed to full-length OMA1, which is consistent with the lower stability of s-OMA1 (Zhang et al., 2014). OMA1 and YME1L protein levels are both restored to basal levels following an 18 h recovery from acute CCCP + 2-DG insult indicating a return to homeostasis (Fig. 4E,F). OMA1 and YME1L protein levels also return to normal levels in vivo following recovery from acute HI injury (Baburamani et al., 2015). Apart from OMA1 degradation, other factors could also influence OMA1-dependent OPA1 processing during recovery from CCCP + 2-DG pretreatment such as reductions in OMA1 protease activity afforded by restoration of the membrane potential, slowed OPA1 biosynthesis (Frezza et al., 2006; Patten et al., 2014), or posttranslational modifications of OMA1 and/or OPA1 (Samant et al., 2014).

The results shown in Fig. 4 indicate that the differential stress-induced degradation of YME1L and OMA1 influences OPA1 proteolytic processing during recovery from acute stress. This suggests that the differential degradation of these proteases alters mitochondrial inner membrane proteolytic activity and can affect aspects of mitochondrial biology such as the regulation of mitochondrial morphology.

## Concluding Remarks

Here, we show that YME1L and OMA1 are reciprocally degraded in response insults that depolarize mitochondria in a process dictated by cellular energetic status. This likely reflects conformational alterations induced by reduced nucleotide levels and/or membrane depolarization that render YME1L or OMA1 susceptible to degradation (Baker et al., 2014; Rainbolt et al., 2015; Zhang et al., 2014). The differential degradation of YME1L and OMA1 can influence aspects of mitochondrial biology such as recovery of tubular

mitochondrial morphology following acute insults. This regulation of mitochondrial morphology can profoundly alter mitochondrial function. Tubular mitochondria are associated with enhanced ETC activity, protection from mitophagy, and desensitization to apoptotic insult (Cribbs and Strack, 2007; Gomes et al., 2011; Rambold et al., 2011; Tondera et al., 2009). Alternatively, fragmented mitochondria have reduced ETC activity, are more susceptible to mitophagy, and are associated with apoptosis (Landes and Martinou, 2011; Twig et al., 2008; Westermann, 2012). Thus, the ability to influence mitochondrial morphology through the differential stress-sensitivity of OMA1 and YME1L provides a mechanism for cells to adjust mitochondrial function to distinct types of stress. The differential, reciprocal degradation of YME1L and OMA1 can also influence other aspects of mitochondrial function regulated by these proteases including mitochondrial protein import, degradation of oxidatively damaged proteins, and BAX/BAK-induced cytochrome c release (Jiang et al., 2014; Rainbolt et al., 2013; Rainbolt et al., 2015; Stiburek et al., 2012).

Imbalances in YME1L and OMA1 activity afforded by their differential degradation could also contribute to mitochondrial dysfunction observed in human diseases. For example, in vivo models of neonatal HI injury that depolarize mitochondria and deplete cellular ATP show increases in OPA1 processing and alterations in mitochondria morphology (Baburamani et al., 2015). Our results would suggest that these effects could be attributed to imbalances in the stress-dependent regulation of YME1L and OMA1 resulting in YME1L degradation and the stabilization of activated OMA1. Consistent with this prediction, YME1L levels are reduced and OMA1 is stabilized in these HI models suggesting that imbalances in the reciprocal degradation of these proteases contribute to the observed mitochondria dysfunction (Baburamani et al., 2015). *OMA1* deletion also rescues mitochondrial defects induced by *YME1L* depletion both in vitro and in vivo, further suggesting that imbalances in the reciprocal regulation of these proteases disrupts mitochondrial biology (Anand et al., 2014; Wai et al., 2015).

Mitochondrial depolarization and metabolic stress are implicated in the onset and pathology of many diseases including neurodegenerative disorders and cardiovascular disease (Nunnari and Suomalainen, 2012; Quiros et al., 2015; Rugarli and Langer, 2012). Chronically such conditions would favor the loss of YME1L and promote the stabilization of active OMA1. This could induce pathologic changes in mitochondrial function associated with these diseases. Thus, our identification of the reciprocal degradation of YME1L and OMA1 reveals a regulatory mechanism to adapt mitochondria function to specific insults and whose imbalance could contribute to the pathologic mitochondria dysfunction observed in diverse diseases.

## EXPERIMENTAL PROCEDURES

### Cellular Lysate Preparation and Immunoblotting

Whole cell lysates were prepared in Lysis Buffer (20 mM HEPES [pH 7.4], 100 mM NaCl, 1 mM EDTA, 1% Triton X-100 supplemented with EDTA-free protease inhibitors [Roche]). Protein concentration in lysates was normalized using the Bio-Rad protein assay. Lysates were separated by electrophoresis on Tris-glycine gels and transferred onto nitrocellulose membranes (Bio-Rad) for immunoblotting. Membranes were blocked and then incubated

with the indicated primary antibodies and visualized following incubation with appropriate IR-Dye conjugated secondary antibodies using the Odyssey Infrared Imaging System (LI-COR Biosciences). Quantification was carried out with LI-COR Image Studio software.

### [$^{35}$S] Metabolic Labeling and Immunoprecipitation

Cells were metabolically labeled with 110 μCi/ml EasyTag EXPRESS$^{35}$S Protein Labeling Mix (PerkinElmer) in DMEM without cysteine and methionine (Corning-Cellgro) supplemented with 10% dialyzed FBS, 2 mM L-glutamine, 100 U ml$^{-1}$ penicillin and 100 μg ml$^{-1}$ streptomycin. After treatment as indicated, cells were washed and recovered in the labeling media for 6 hours. Following labeling, lysates were prepared in Lysis buffer and denatured with 1% SDS by boiling for 5 min at 100°C. Denatured lysates were diluted 10 fold into RIPA Buffer without SDS (50 mM Tris [pH 7.5], 150 mM NaCl, 0.5% sodium deoxycholate, 1% Triton X-100) and pre-cleared by incubation with sepharose 4B beads (Sigma). OPA1 was immunoprecipitated with OPA1 antibody (BD Transduction Labs) conjugated to protein G sepharose beads (Life Technologies). The beads were washed four times in RIPA buffer and labeled OPA1 was eluted by boiling in 6x Laemmli buffer, separated by SDS-PAGE, and imaged by autoradiography using a Typhoon Trio Imager (GE Healthcare). Densitometry analysis of autoradiograms was carried out with Fiji ImageJ software. The fraction of OPA1 isoforms was calculated using the equation: [$^{35}$S]-labeled OPA1 isoform / total [$^{35}$S]-labeled OPA1.

### Statistical Analysis

Data are presented as mean ± SEM and were analyzed by Student's t-test to determine significance.

## Supplementary Material

Refer to Web version on PubMed Central for supplementary material.

## Acknowledgments

We thank Alexander van der Bliek (UCLA) for providing OMA1$^{HA}$ plasmid; Danling Wang and Peter Schultz (TSRI) for providing $^{mt}$GFP MEFs; Sylvia Neumann (UCLA), Jaclyn Saunders, George Campbell, and Romain Chassefeyre (TSRI) for helpful discussions; and Eros Lazzerini Denchi (TSRI) for microscopy time. This work was supported by the NIH (DK102635 and NS092829), the Ellison Medical Foundation, and the Amyloidosis Foundation. JL was supported by a George Hewitt Foundation postdoctoral fellowship.

## References

Anand R, Langer T, Baker MJ. Proteolytic control of mitochondrial function and morphogenesis. Biochim Biophys Acta. 2013; 1833:195–204. [PubMed: 22749882]

Anand R, Wai T, Baker MJ, Kladt N, Schauss AC, Rugarli E, Langer T. The i-AAA protease YME1L and OMA1 cleave OPA1 to balance mitochondrial fusion and fission. J Cell Biol. 2014; 204:919–929. [PubMed: 24616225]

Baburamani AA, Hurling C, Stolp H, Sobotka K, Gressens P, Hagberg H, Thornton C. Mitochondrial Optic Atrophy (OPA) 1 Processing Is Altered in Response to Neonatal Hypoxic-Ischemic Brain Injury. Int J Mol Sci. 2015; 16:22509–22526. [PubMed: 26393574]

Baker MJ, Lampe PA, Stojanovski D, Korwitz A, Anand R, Tatsuta T, Langer T. Stress-induced OMA1 activation and autocatalytic turnover regulate OPA1-dependent mitochondrial dynamics. EMBO J. 2014; 33:578–593. [PubMed: 24550258]

Bohovych I, Fernandez MR, Rahn JJ, Stackley KD, Bestman JE, Anandhan A, Franco R, Claypool SM, Lewis RE, Chan SS, et al. Metalloprotease OMA1 Fine-tunes Mitochondrial Bioenergetic Function and Respiratory Supercomplex Stability. Scientific reports. 2015; 5:13989. [PubMed: 26365306]

Chan DC. Fusion and fission: interlinked processes critical for mitochondrial health. Annu Rev Genet. 2012; 46:265–287. [PubMed: 22934639]

Cribbs JT, Strack S. Reversible phosphorylation of Drp1 by cyclic AMP-dependent protein kinase and calcineurin regulates mitochondrial fission and cell death. EMBO Rep. 2007; 8:939–944. [PubMed: 17721437]

Desmurs M, Foti M, Raemy E, Vaz FM, Martinou JC, Bairoch A, Lane L. C11orf83, a mitochondrial cardiolipin-binding protein involved in bc1 complex assembly and supercomplex stabilization. Mol Cell Biol. 2015; 35:1139–1156. [PubMed: 25605331]

Frezza C, Cipolat S, Martins de Brito O, Micaroni M, Beznoussenko GV, Rudka T, Bartoli D, Polishuck RS, Danial NN, De Strooper B, et al. OPA1 controls apoptotic cristae remodeling independently from mitochondrial fusion. Cell. 2006; 126:177–189. [PubMed: 16839885]

Gomes LC, Di Benedetto G, Scorrano L. During autophagy mitochondria elongate, are spared from degradation and sustain cell viability. Nat Cell Biol. 2011; 13:589–598. [PubMed: 21478857]

Ishihara N, Fujita Y, Oka T, Mihara K. Regulation of mitochondrial morphology through proteolytic cleavage of OPA1. EMBO J. 2006; 25:2966–2977. [PubMed: 16778770]

Jiang X, Jiang H, Shen Z, Wang X. Activation of mitochondrial protease OMA1 by Bax and Bak promotes cytochrome c release during apoptosis. Proc Natl Acad Sci U S A. 2014; 111:14782–14787. [PubMed: 25275009]

Landes T, Martinou JC. Mitochondrial outer membrane permeabilization during apoptosis: the role of mitochondrial fission. Biochim Biophys Acta. 2011; 1813:540–545. [PubMed: 21277336]

Li H, Ruan Y, Zhang K, Jian F, Hu C, Miao L, Gong L, Sun L, Zhang X, Chen S, et al. Mic60/Mitofilin determines MICOS assembly essential for mitochondrial dynamics and mtDNA nucleoid organization. Cell Death Differ. 2015

Mishra P, Carelli V, Manfredi G, Chan DC. Proteolytic cleavage of Opa1 stimulates mitochondrial inner membrane fusion and couples fusion to oxidative phosphorylation. Cell Metab. 2014; 19:630–641. [PubMed: 24703695]

Nunnari J, Suomalainen A. Mitochondria: in sickness and in health. Cell. 2012; 148:1145–1159. [PubMed: 22424226]

Patten DA, Wong J, Khacho M, Soubannier V, Mailloux RJ, Pilon-Larose K, MacLaurin JG, Park DS, McBride HM, Trinkle-Mulcahy L, et al. OPA1-dependent cristae modulation is essential for cellular adaptation to metabolic demand. EMBO J. 2014; 33:2676–2691. [PubMed: 25298396]

Quiros PM, Langer T, Lopez-Otin C. New roles for mitochondrial proteases in health, ageing and disease. Nat Rev Mol Cell Biol. 2015; 16:345–359. [PubMed: 25970558]

Quiros PM, Ramsay AJ, Sala D, Fernandez-Vizarra E, Rodriguez F, Peinado JR, Fernandez-Garcia MS, Vega JA, Enriquez JA, Zorzano A, et al. Loss of mitochondrial protease OMA1 alters processing of the GTPase OPA1 and causes obesity and defective thermogenesis in mice. EMBO J. 2012; 31:2117–2133. [PubMed: 22433842]

Rainbolt TK, Atanassova N, Genereux JC, Wiseman RL. Stress-regulated translational attenuation adapts mitochondrial protein import through Tim17A degradation. Cell Metab. 2013; 18:908–919. [PubMed: 24315374]

Rainbolt TK, Saunders JM, Wiseman RL. YME1L degradation reduces mitochondrial proteolytic capacity during oxidative stress. EMBO Rep. 2015; 16:97–106. [PubMed: 25433032]

Rambold AS, Kostelecky B, Elia N, Lippincott-Schwartz J. Tubular network formation protects mitochondria from autophagosomal degradation during nutrient starvation. Proc Natl Acad Sci U S A. 2011; 108:10190–10195. [PubMed: 21646527]

Rugarli EI, Langer T. Mitochondrial quality control: a matter of life and death for neurons. EMBO J. 2012; 31:1336–1349. [PubMed: 22354038]

Samant SA, Zhang HJ, Hong Z, Pillai VB, Sundaresan NR, Wolfgeher D, Archer SL, Chan DC, Gupta MP. SIRT3 deacetylates and activates OPA1 to regulate mitochondrial dynamics during stress. Mol Cell Biol. 2014; 34:807–819. [PubMed: 24344202]

Song Z, Chen H, Fiket M, Alexander C, Chan DC. OPA1 processing controls mitochondrial fusion and is regulated by mRNA splicing, membrane potential, and Yme1L. J Cell Biol. 2007; 178:749–755. [PubMed: 17709429]

Stiburek L, Cesnekova J, Kostkova O, Fornuskova D, Vinsova K, Wenchich L, Houstek J, Zeman J. YME1L controls the accumulation of respiratory chain subunits and is required for apoptotic resistance, cristae morphogenesis, and cell proliferation. Mol Biol Cell. 2012; 23:1010–1023. [PubMed: 22262461]

Tondera D, Grandemange S, Jourdain A, Karbowski M, Mattenberger Y, Herzig S, Da Cruz S, Clerc P, Raschke I, Merkwirth C, et al. SLP-2 is required for stress-induced mitochondrial hyperfusion. EMBO J. 2009; 28:1589–1600. [PubMed: 19360003]

Twig G, Elorza A, Molina AJ, Mohamed H, Wikstrom JD, Walzer G, Stiles L, Haigh SE, Katz S, Las G, et al. Fission and selective fusion govern mitochondrial segregation and elimination by autophagy. EMBO J. 2008; 27:433–446. [PubMed: 18200046]

Wai T, Garcia-Prieto J, Baker MJ, Merkwirth C, Benit P, Rustin P, Ruperez FJ, Barbas C, Ibanez B, Langer T. Imbalanced OPA1 processing and mitochondrial fragmentation cause heart failure in mice. Science. 2015; 350:aad0116. [PubMed: 26785494]

Westermann B. Bioenergetic role of mitochondrial fusion and fission. Biochim Biophys Acta. 2012; 1817:1833–1838. [PubMed: 22409868]

Zhang K, Li H, Song Z. Membrane depolarization activates the mitochondrial protease OMA1 by stimulating self-cleavage. EMBO Rep. 2014; 15:576–585. [PubMed: 24719224]

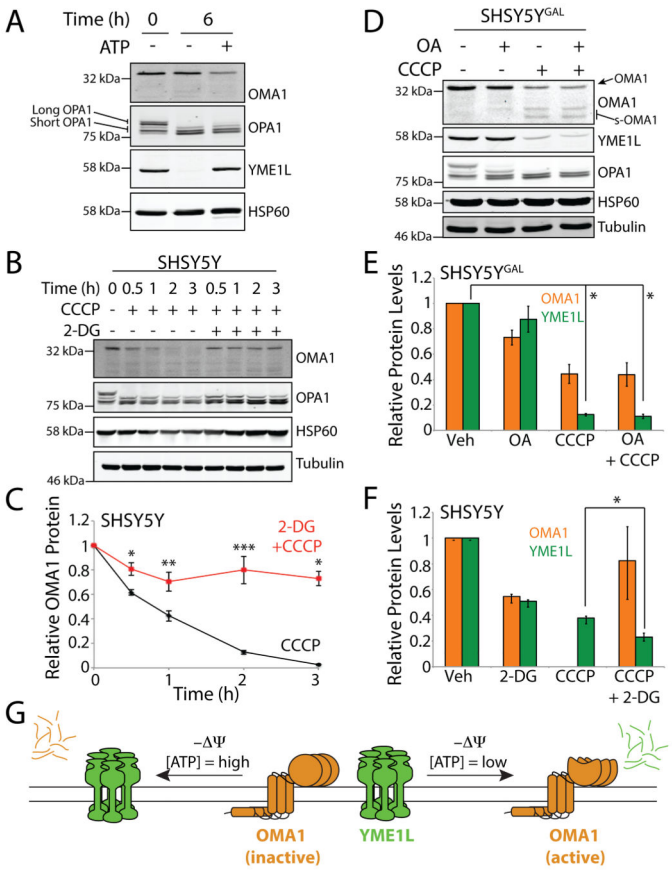


**Figure 1. Membrane depolarization-induced OMA1 degradation requires ATP**

**A.** Immunoblot of mitochondria isolated from SHSY5Y cells incubated with or without ATP (5 mM) at 37°C for 6 hours, as indicated.

**B.** Representative immunoblot of lysates from SHSY5Y cells treated with CCCP (25 μM) alone or with 2-deoxy-D-glucose (2-DG, 10 mM) for the indicated time.

**C.** Quantification of normalized OMA1 protein levels from immunoblots as depicted in Fig. 1B. Error bars show SEM for n=3. *p<0.05, **p<0.01, ***p<0.001

**D.** Immunoblot of lysates prepared from SHSY5Y cells cultured in galactose-supplemented media treated with oligomycin A (OA, 5 nM) and/or CCCP (50 μM) for 6 h.

**E.** Quantification of normalized OMA1 and YME1L protein levels from immunoblots as shown in Fig. 1D. Error bars show SEM for n=3. *p<0.05

**F.** Quantification of normalized OMA1 and YME1L protein levels from immunoblots as shown in Fig. S1G. Error bars show SEM for n=4. *p<0.05

**G.** Illustration showing the differential degradation of YME1L and OMA1 induced by membrane depolarization in the presence or absence of ATP.

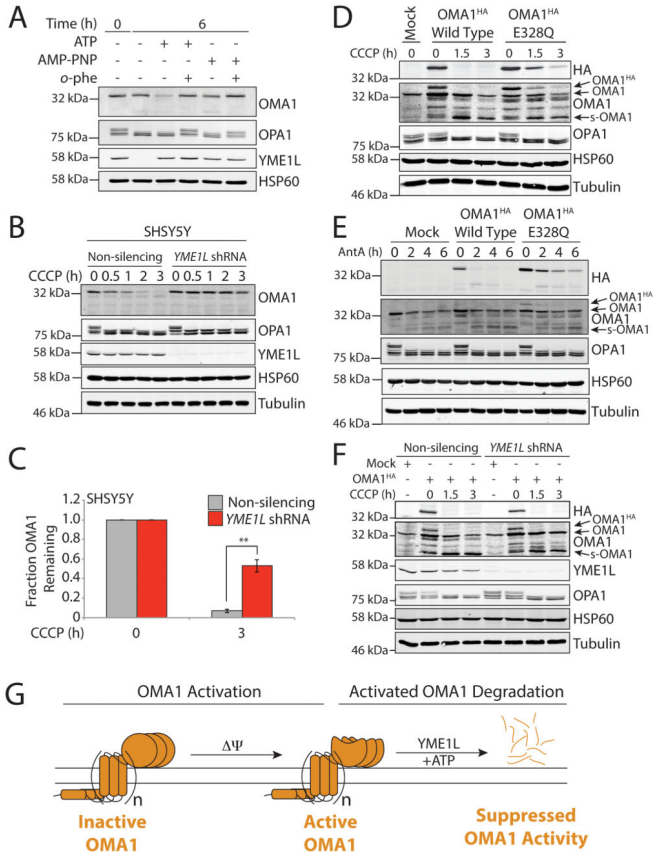


**Figure 2. OMA1 degradation requires ATP-dependent YME1L activity**

**A.** Immunoblot of mitochondria isolated from SHSY5Y cells incubated with ATP (5 mM), AMP-PNP (5 mM) and/or *o*-phenanthroline (*o*-phe, 1 mM), as indicated at 37°C for 6 hours.

**B.** Immunoblot of lysates prepared from SHSY5Y cells expressing non-silencing or *YME1L* shRNA treated with CCCP (25 μM) for the indicated time.

**C.** Quantification of normalized OMA1 protein levels from immunoblots as shown in Fig. 2B. Data were normalized to t=0 h for each shRNA respectively. Error bars show SEM for n=5. **p<0.01.

**D.** Immunoblot of lysates prepared from SHSY5Y cells transfected with wild type $OMA1^{HA}$ or the E328Q $OMA1^{HA}$ treated with CCCP (25 μM) for the indicated time.

**E.** Immunoblot of lysates prepared from SHSY5Y cells cultured in galactose-supplemented media expressing wild type $OMA1^{HA}$ or E328Q $OMA1^{HA}$ treated with antimycin A (100 nM) for the indicated time.

**F.** Immunoblot of lysates prepared from SHSY5Y cells expressing non-silencing or *YME1L* shRNA, transfected with $OMA1^{HA}$ and treated with CCCP (25 μM) for the indicated time.

**G.** Illustration showing the proposed two-step mechanism of stress-induced OMA1 activation and degradation. Membrane depolarization activates the OMA1 protease, allowing rapid processing of OMA1 substrates such as OPA1. Active OMA1 is then degraded by the ATP-dependent activity of YME1L suppressing OMA1 proteolytic activity.

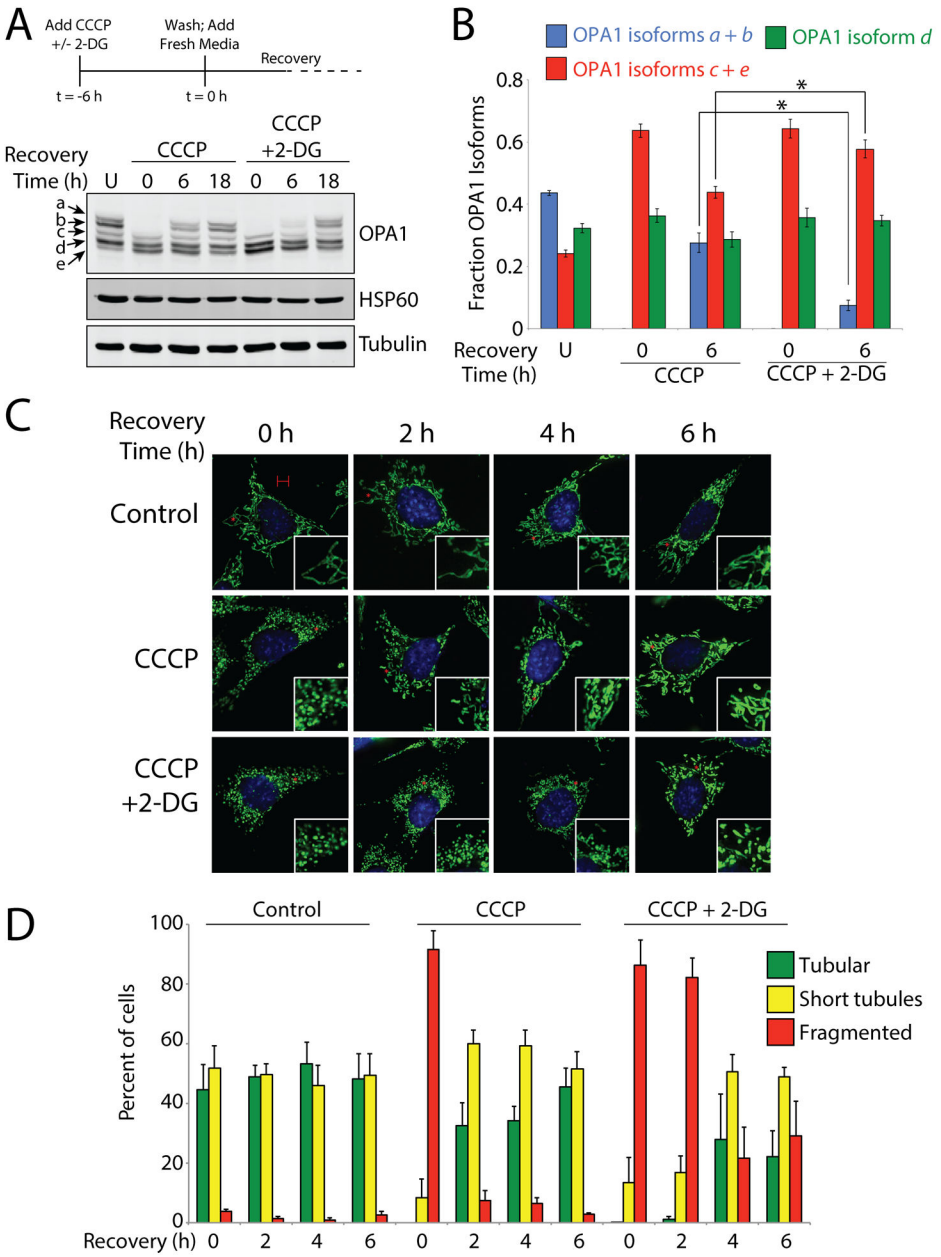


**Figure 3. ATP depletion slows the recovery of tubular mitochondrial morphology following membrane depolarization induced fragmentation**

**A.** Representative immunoblot of lysates prepared from SHSY5Y cells pretreated with 2-deoxy-D-glucose (2-DG; 10 mM) and/or CCCP (25 μM) for 6 h, washed, and recovered for the indicated times. An untreated control (U) is also shown. The experimental protocol is shown above.

**B.** Quantification of OPA1 isoforms from immunoblots as shown in Fig. 3A. Error bars depict SEM for n=4. *p<0.05.

**C.** Representative images of MEFs stably expressing $^{mt}$GFP treated with 2-DG (10 mM) and/or CCCP (25 μM) as indicated for 2 hours, washed, and recovered for the indicated

times. Scale bar indicates 5 μm. Red asterisks mark the center of the expanded region shown.

**D.** Quantification of mitochondria morphology in cells (n≥40 cells per condition) from images as depicted in Fig. 3C. Error bars depict SEM from n=3 biologic replicates.

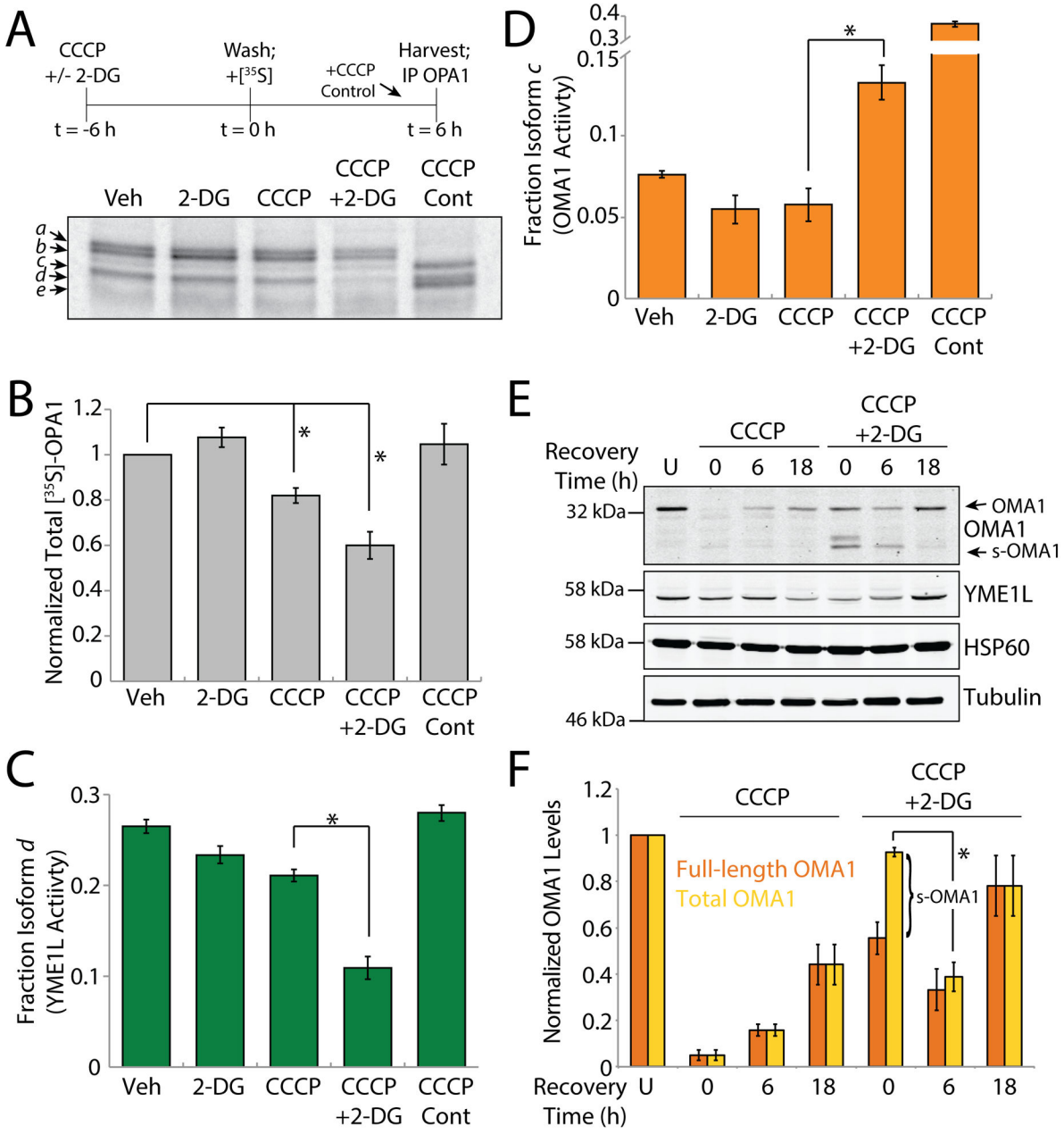


**Figure 4. OPA1 Processing is Altered During Recovery from Membrane Depolarization and ATP Depletion**

**A.** Representative autoradiogram of newly synthesized [$^{35}$S]-OPA1 immunopurified from SHSY5Y cells pretreated for 6 h with 2-deoxy-D-glucose (2-DG, 10 mM) and/or CCCP (25 μM) as indicated. The labeling protocol is shown above. Arrows identify the different OPA1 isoforms.

**B.** Quantification of total newly synthesized [$^{35}$S]-OPA1 from autoradiograms as shown in Fig. 4A. Error bars show SEM for n=4. *p<0.05

**C.** Quantification of fraction OPA1 isoform *d* (produced by YME1L activity) from autoradiograms as shown in Fig. 4A. Error bars show SEM for n=4. *p<0.05

**D.** Quantification of fraction OPA1 isoform *c* (produced by OMA1 activity) from autoradiograms as shown in Fig. 4A. Error bars show SEM for n=4. *p<0.05

**E.** Representative immunoblot of lysates from SHSY5Y cells pretreated with 2-DG (10 mM) and/or CCCP (25 μM) for 6 h and allowed to recover for the indicated time. The experimental protocol used for this experiment is analogous to that shown in Fig. 3A.

**F.** Quantification of normalized full-length and total (full-length OMA1 + s-OMA1) OMA1 protein levels from immunoblots as shown in Fig. 4E. The amount of s-OMA1 is reflected by the difference in full-length and total OMA1 as depicted. Error bars show SEM for n=4. *p<0.05.